AIP | Journal of Applied Physics

Oscillation dynamics of embolic microspheres in flows with red blood cell suspensions

Tamal Das, Dario Carugo, Xunli Zhang, and Suman Chakraborty

Citation: J. Appl. Phys. **112**, 124701 (2012); doi: 10.1063/1.4768889
View online: http://dx.doi.org/10.1063/1.4768889
View Table of Contents: http://jap.aip.org/resource/1/JAPIAU/v112/i12
Published by the American Institute of Physics.

Related Articles

Why and how does collective red blood cells motion occur in the blood microcirculation?
Phys. Fluids 24, 101901 (2012)

Depletion layer formation in suspensions of elastic capsules in Newtonian and viscoelastic fluids
Phys. Fluids 24, 061902 (2012)

Separation of blood cells using hydrodynamic lift
Appl. Phys. Lett. 100, 183701 (2012)

A new laser Doppler flowmeter prototype for depth dependent monitoring of skin microcirculation
Rev. Sci. Instrum. 83, 034302 (2012)

Vesicle tumbling inhibited by inertia
Phys. Fluids 24, 031901 (2012)

Additional information on J. Appl. Phys.

Journal Homepage: http://jap.aip.org/
Journal Information: http://jap.aip.org/about/about_the_journal
Top downloads: http://jap.aip.org/features/most_downloaded
Information for Authors: http://jap.aip.org/authors

ADVERTISEMENT

Downloaded 18 Dec 2012 to 152.78.177.66. Redistribution subject to AIP license or copyright; see http://jap.aip.org/about/rights_and_permissions

Oscillation dynamics of embolic microspheres in flows with red blood cell suspensions

Tamal Das,[1,a)] Dario Carugo,[2] Xunli Zhang,[2] and Suman Chakraborty[3,b)]
[1]*Department of Biotechnology, Indian Institute of Technology Kharagpur, Kharagpur 721302, India*
[2]*Bioengineering Group, Faculty of Engineering and the Environment, University of Southampton, Southampton SO17 1BJ, United Kingdom*
[3]*Department of Mechanical Engineering, Indian Institute of Technology Kharagpur, Kharagpur 721302, India*

(Received 10 September 2012; accepted 6 November 2012; published online 18 December 2012)

Dynamic nature of particle motion in blood flow is an important determinant of embolization based cancer therapy. Yet, the manner in which the presence of high volume fraction of red blood cells influences the particle dynamics remains unknown. Here, by investigating the motions of embolic microspheres in pressure-driven flows of red blood cell suspensions through capillaries, we illustrate unique oscillatory trends in particle trajectories, which are not observable in Newtonian fluid flows. Our investigation reveals that such oscillatory behavior essentially manifests when three simultaneous conditions, namely, the Reynolds number beyond a threshold limit, degree of confinement beyond a critical limit, and high hematocrit level, are fulfilled simultaneously. Given that these conditions are extremely relevant to fluid dynamics of blood or polymer flow, the observations reported here bear significant implications on embolization based cancer treatment as well as for complex multiphase fluidics involving particles. © *2012 American Institute of Physics*. [http://dx.doi.org/10.1063/1.4768889]

I. INTRODUCTION

Velocity distributions and trajectories of suspended particles have been thought to dictate the efficacy of a major anti-cancer treatment method called embolization therapy.[1–5] Embolization is defined as a process by which the blood vessels close to tumor site can be blocked with micron sized particles in order to cut off the local nutrient supply or to deliver therapeutic chemicals (chemoembolization) and radioactive materials (radioembolization) for destruction of cancer cells in a site specific manner.[2,6–8] With the advent of narrow catheters with diameters close to 1 mm, embolization therapy has been perceived to be a major protocol towards minimal incision strategy.[9,10] To facilitate the embolization process, microparticles such as spherical microbeads or microspheres are employed.[7,11] Injected through catheters, these microspheres are transported with the blood flow and form the blockage at a point where vasculature diameter is smaller than the bead diameter. Despite its immense promises, embolization therapy currently suffers from lack of accurate spatial preconception of the blocking site,[5,12] offering concerning challenges to the research community.

Embolic microspheres are commonly synthesized by colloidal processes which result in Gaussian distributed size ranges with desired mean diameters (e.g., 200 μm) and different standard deviations depending on the process control.[11] Considering this variability in microsphere diameters (d_p), the blockage may be predicted as a function of the particle velocity (v_p) distribution (in the sense that injected simultaneously, the fastest particle determines the blockage point) under appropriate fluidic conditions. A list of such conditions should then include the transport regime of arterial blood flow, finite confinement effect of the blood vessels, and non-Newtonian effects dictated by the volume fractions of suspended red blood cells (RBCs). Unfortunately, no effort has been made to investigate particle dynamics in these physiologically relevant conditions, which has significantly impeded the progress of embolization therapy. It is worthwhile to mention in this context that in addition to the consideration of the background flow behavior to be following the classical Newtonian paradigm, non-trivialities with regard to confinement effects have been grossly overlooked.[13–17]

Axial and lateral translations of suspended particles in inertial yet Newtonian fluid flow are amenable to matched-asymptotic analysis if particle diameters are infinitesimally small compared to the channel diameter (d_c), i.e., relative particle diameter $\alpha = d_p/d_c \ll 1$, essentially implicating the considerations of particles as point masses. However, for microspheres ($d_p = 100$–$300\,\mu$m) translating within small arteries ($d_c \sim 1$ mm),[1,3,6,10] confinement effects dictated by finite values of α may turn out to be critical in determining the particle dynamics. Relevantly, for Newtonian fluid flows through narrow confinements, the cross-stream particle migration at inertial Reynolds number (Re) regimes has been analyzed and engineered towards microfluidic particle separator design and optimization.[14,18–21] Yet, it remains little understood whether experimental and theoretical predictions based on Newtonian flow can also be extrapolated to non-Newtonian cases. Investigations prove that such extrapolations could be inappropriate and what they effectively provide is a glimpse of non-intuitive dynamics such as transverse instability of lateral motion that arises when one attempts to characterize particle trajectory in pressure-driven

[a)]Present address: Max Planck Institute for Intelligent Systems, Stuttgart 70569, Germany.
[b)]Author to whom correspondence should be addressed. Electronic mail: suman@mech.iitkgp.ernet.in.

 © 2012 American Institute of Physics

Downloaded 18 Dec 2012 to 152.78.177.66. Redistribution subject to AIP license or copyright; see http://jap.aip.org/about/rights_and_permissions

viscoelastic fluid flows.[22,23] They, however, have not flushed out relevant dimensionless parameters dictating the possibilities of oscillatory dynamical characteristics, and have rather advocated for case-specific analysis.

Here, we investigate the velocity distributions and particle trajectories of embolic microspheres within capillaries and most importantly, in the presence of RBCs, so that essential information can be obtained about particle dynamics in RBC suspensions in physiologically relevant Re and α regimes. Subsequently, we report that a unique lateral oscillatory behavior in the particle dynamics may be observed if the experimental parameters correspond to Reynolds numbers (Re) and the confinement parameter (α) beyond critical limits, with high hematocrit levels prevailing simultaneously. Following, in Sec. II, we describe the experimental protocol. Then, in Sec. III, we delineate the important results, pin down important parameters and qualitatively analyze the dynamics of lateral oscillation for its probable governing mechanics. In Sec. IV, we summarize the important conclusions from our study.

II. MATERIALS AND METHODS

Contrast agent ($\rho = 1.3$ mg/ml) was mixed with phosphate buffered saline (PBS, pH = 7.4, $\rho = 1.0$ mg/ml) so as to obtain uniform density ($\rho = 1.1$ mg/ml) of embolic microbeads (Bead Block, Biocompatibles UK Ltd., UK) (i.e., bead suspension). Beads of size range 100–300 μm (normal distribution; mean $d_p = 200\,\mu$m, standard deviation $\sigma = 100\,\mu$m) were suspended in the uniform density solution. Bead suspension was then added to a concentrated suspension of rat red blood cells in plasma. RBCs were suspended in such a volumetric ratio as to correspond to a chosen hematocrit level (volume percentage).

The number density of the beads was adjusted such that, within the flow-field, inter-bead distances remained large enough to eliminate mutual hydrodynamic interactions. For hydrodynamic studies, fluid containing embolic beads was driven by a syringe pump at pre-set volumetric flow rates through a length of cylindrical glass tube with a diameter (d_c) of 1.1 mm (Fig. 1). A selected length-segment of the circular tube was subjected to observation under an inverted microscope (10× objective, IX-71, Olympus) (Fig. 1). To ensure that all measurements were taken in equilibrium positions of the particles with respect to their transverse motion, two relevant lengths were estimated, which played important roles in the design of the experimental set-up. At first, for each Reynolds number, the entrance length (l_e) was estimated. l_e is the distance between the inflow end of the capillary and the point from which the fully developed flow starts. In laminar flow regime, it is estimated as $l_e = 0.06 d_c Re$, which in the range of $Re = 10 - 30$ was calculated to be between 0.66 and 1.98 mm. Next, the distance required to establish transverse equilibrium position under lateral lift was estimated. Following previous reports on flow focusing,[15–17] this parameter was denoted by l_f and was related to channel diameter and Reynolds number as $l_f/d_c \approx 6\pi A^{-1}\mathrm{Re}^{-1}(d_c/d_p)^3$. Accordingly, the total distance between the inflow end of the capillary and point of observation (l_o) was fixed in a way such that $l_o > l_e + l_f$. In most conservative estimation, we maintained $l_o \geq 10 \times (l_e + l_f)$ to ensure that equilibrium was indeed achieved.

For each run (e.g., fixed flow set-up, flow rate, other experimental condition), series of 100 image-frames were captured sequentially with a time interval of 20 ms between subsequent frames. Bead velocities were determined by quantifying the bead-displacement over subsequent frames using a micro particle tracking velocimetry (μPTV) technique. Bead positions across the channel cross-section were also determined. Towards this, microscope focus was first set in the middle plane of the cross-section and images were taken (Fig. 1). Notably, in Fig. 1, U_m conforms to the maximum velocity, which may be estimated from the information of the average velocity, based on constitutive non-Newtonian behavior. Here, we employed a Power Law model,[24,25] based on the considerations outlined in the supplementary material.[26]

During post-processing, bead-images were analyzed by an indigenously developed image processing program (MATLAB, MathWorks) and the sharpness of the bead edge was determined. Only in the case that the edge sharpness was found to be beyond a critical limit, the bead was considered to be in-focal-plane and positional information was obtained. This method enabled the determination of bead position

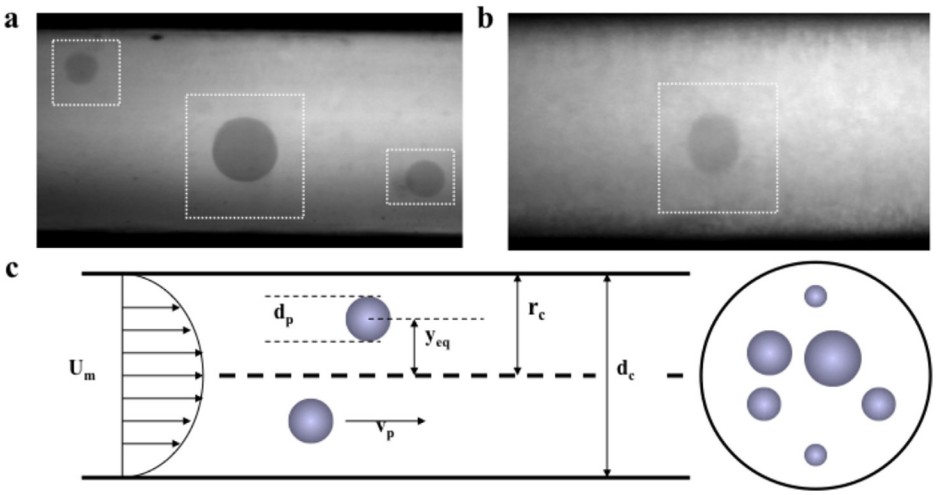

FIG. 1. Schematic depiction of the problem. Representative images of embolic beads in the absence (a) and in the presence (b) of red blood cells. (c) Geometric delineation of the problem.

Downloaded 18 Dec 2012 to 152.78.177.66. Redistribution subject to AIP license or copyright; see http://jap.aip.org/about/rights_and_permissions

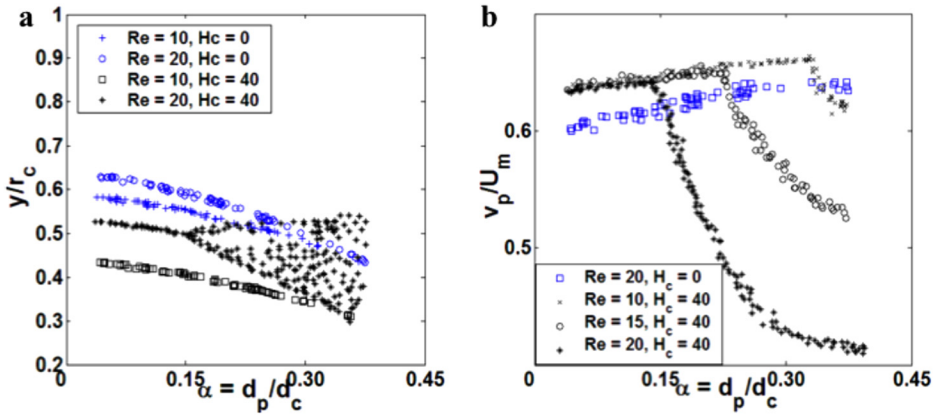

FIG. 2. Migration of embolic microspheres in the presence or absence of red blood cells as obtained from experiments. (a) Lateral positions (equilibrium and oscillatory) and (b) axial velocities of microspheres as the function of relative particle diameter (α).

distribution without the requirement of expensive laser scanning confocal microscope based visualization system.

Particle oscillations were detected by two means, namely, the number ensemble (Fig. 2) and the time ensemble method (Fig. 3(a)). In number ensemble method, we fixed the region of observation and counted how many in-focus beads passed through that region. We then determined the size-distribution of the beads that passed through this region. By changing the position of this region of interest, we finally computed the bead distribution over the whole observed area of the channel. To give a step-wise protocol, particle distribution at a fixed cross-section of the capillary was determined. Particles for which focus was found to be sufficiently sharp, by analyzing the edge of the particles,[26] were registered for their y-axis location. In non-oscillatory condition, as reported by others,[13,14] this measurement should ideally result in a single y-point for a fixed particle diameter. In oscillatory condition, however, single y-point would cease to exist. Instead, a distribution of y-points for a fixed particle would develop. This is equivalent to the process of recording the positions of particles at different phases, which are nevertheless going through oscillatory motion of same frequency and amplitude. The number ensemble method provides the statistics of the particle oscillation.

In time ensemble method, we recorded the y-position of each bead individually, from the time-series images, as it passed though observation area of the channel. We, however, discarded those y-positions, for which bead was not in focus. To give a step-wise protocol, y-position of a single particle was recorded within the microscope field as it is surfaced into prominent focus.[26] Likewise, in all cases, particle-focus was evaluated at each frame and particle position was recorded only when it was in focus. Then, superimposing several of those corresponding to a fixed particle diameter, the characteristic oscillatory motion was delineated (Fig. 3(a)). The time ensemble method provides dynamic details of the particle oscillation.

III. RESULTS AND DISCUSSION

In order to bench-mark our visualization scheme with previous reports, we have first examined the statistics of particle dynamics in the absence of RBCs. Two forms of important behavior emerge here. First, in the inertial range of Reynolds number (2–30), the particles settle into lateral equilibrium positions (y_{eq}) which are found to be a function of the relative particle diameter (α) (Fig. 2). In agreement with the report of Di Carlo *et al.*,[13] y_{eq} has been observed to

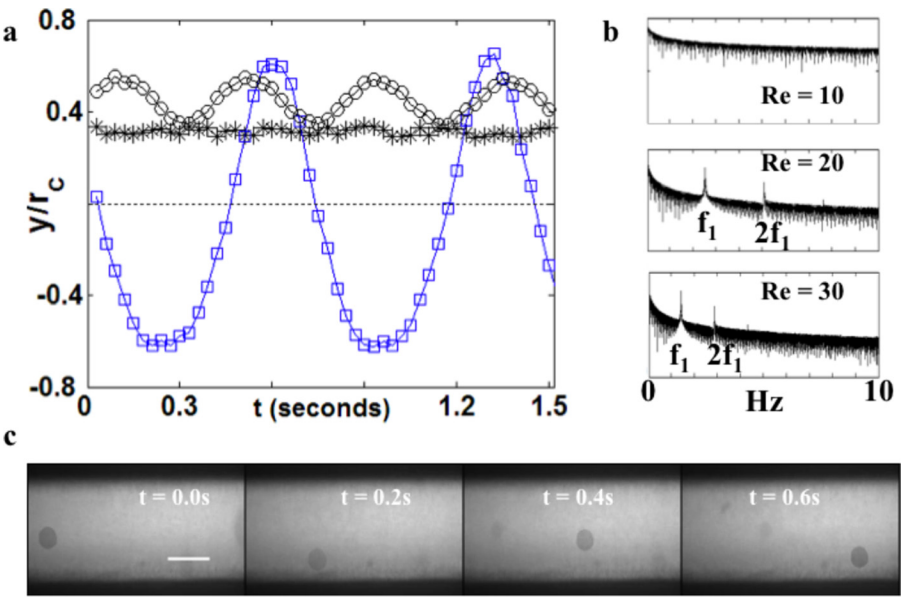

FIG. 3. Experimental variations in dynamic behavior of migrating microspheres. (a) Representative tracks of beads with $\alpha \sim 0.3$ at $Re = 10$ (star); $Re = 20$ (circle); and $Re = 30$ (square). (b) Frequency spectra of averaged bead (with $\alpha \sim 0.3$) tracks at different Reynolds numbers. Y-axis range is 10^{-6} to 1 in log scale. $H_c = 40\%$. (c) Representative image sequence showing bead oscillation (interframe time interval = 200 ms). Scale bar is 400 μm.

Downloaded 18 Dec 2012 to 152.78.177.66. Redistribution subject to AIP license or copyright; see http://jap.aip.org/about/rights_and_permissions

be decreasing with increasing α, which is not inflicted by the direct wall-contact (Fig. 2) but depends upon the attractor location of lift force (f_L) landscape in such confined geometries. Also, relatively small particles ($\alpha \ll 1$) have been noted to settle into the well-known Segré-Silberberg equilibrium position for which $y_{eq} \sim 0.6$.[13,14,27] Second, with the variation in α, the longitudinal particle migration velocity (v_p) remains approximately constant. Such observation consequently vindicates and corroborates with the results of previous experimental investigations.[13,14]

However, introducing RBCs into the flow at 40% hematocrit level (volume percentage) leads to significant change in both y_{eq} and v_p distributions in the α space. At $Re = 10$, y_{eq} for each α shifts towards the channel center. At $Re = 20$, y_{eq} exhibits a similar centripetal shift when $\alpha < 0.15$. However, when $\alpha > 0.15$, y_{eq} ceases to acquire unique values at a given α, and as evident from Fig. 2(a), the distribution of lateral position of beads widens with increasing α. The first form of behavior, i.e., a centripetal shift, may be explained by considering the fact that a modification in the apparent viscosity due to RBCs decreases the lateral flow gradient and hence, the consequent lift force. The second form of observation, however, is unique and may not be explained from trivial fluid dynamics considerations.[22,23] More importantly, it should also be noted that in the presence of RBCs, v_p suddenly decreases when α reaches a critical value at which there occurs no distinctive lateral equilibrium position (Fig. 2(b)). While the particles underwent oscillations in the radial direction, no such oscillation could be detected in longitudinal or axial direction (flow direction), eliminating any splitting in the velocity statistics for a fixed particle diameter. However, as the lateral oscillation would now enforce a helical particle trace in three dimensional space rather than the usual straight-line motion, it would actually reduce the particle velocity in the axial direction. When this effect is prominent, instead of a slightly increasing trend of axial velocity with increasing particle diameter,[15,17] one would see a non-intuitive decrease as in Fig. 2(b), especially for the cases with finite hematocrit level. To the best of our knowledge, such decreasing trend has not been reported for Newtonian fluids (conforming to samples with zero hematocrit levels).

Given that such unique dynamics, nevertheless, are expected to play governing roles in embolization therapy, we have subsequently characterized all of the experimental dynamic behaviors by determining the corresponding frequency spectra. Fast Fourier transform (FFT) was performed on the time-position data, which provided the frequency spectrum. It then emerges that the entire range of experimental data can be categorized into three possible forms of behavior, namely, fixed lateral position, oscillating lateral position but oscillation confined within one half of the channel, and oscillation encompassing both halves (Fig. 3). Fig. 3 depicts the typical dynamic behavior and corresponding frequency spectra for $\alpha = 0.3 \pm 0.03$. From the spectra, fundamental lateral oscillation frequencies at $Re = 20$ and 30 have been found to be 0.26 and 0.15 Hz, respectively (Fig. 3). If extrapolated in three dimensions, the aforementioned oscillation behavior corresponds to helical trajectories of embolic beads, which explains why the effective longitudinal velocity decreases as the oscillatory dynamics sets in.

One needs to note that in relevance to the experimental data presented in Figs. 2 and 3, three interpretations are possible to explain the observations. First, the particles might not have yet reached their radial equilibrium position but would do so further downstream. Second, the particles might reach a radial equilibrium position but the initial range, most likely covering the whole radial range from the center line to the wall, could have contracted to the observed range even further downstream. Finally, the particles might have performed a radial oscillation encompassing the whole radial range observed. We have claimed above that it is the third alternative that is indeed correct. In order to substantiate our proposition, we have systemically isolated the right one by taking the measurement at different positions along the capillary length. Experimental readings have been taken at three different positions, all satisfying the criteria of minimal distance for equilibrium, i.e., $l_o \geq 10 \times (l_e + l_f)$. Subsequently, as it can be observed from Fig. 4, there is no significant change in particle distribution even if acquisitions were made at different longitudinal positions. This result

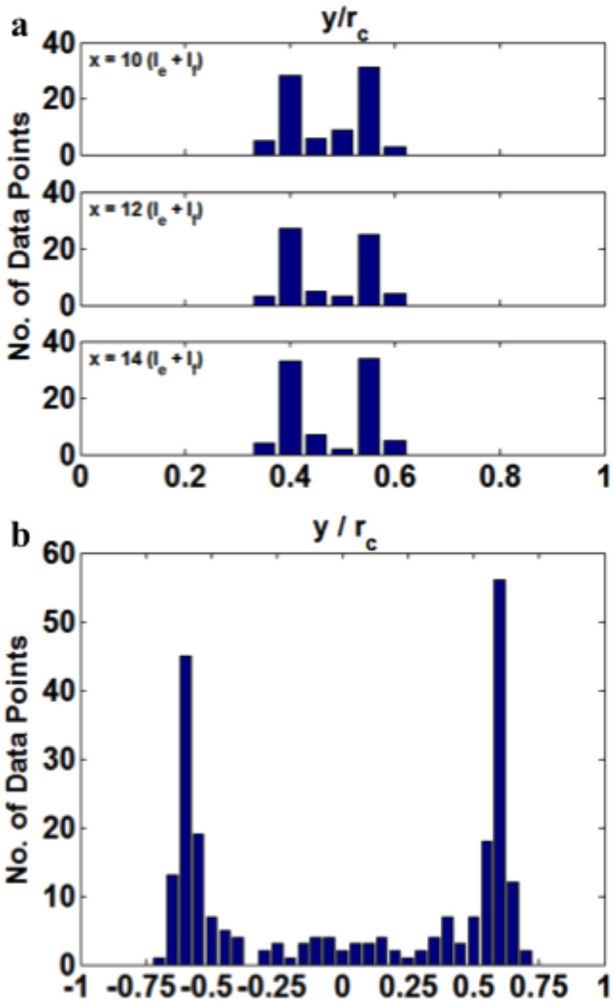

FIG. 4. Number ensemble representation of bead oscillation in capillary. (a) Constancy of statistical distribution of beads ($\alpha \sim 0.3$) along the channel length for $H_c = 40\%$ and $Re = 20$. (b) Statistical distribution of beads ($\alpha \sim 0.3$) for $H_c = 40\%$ and $Re = 30$.

Downloaded 18 Dec 2012 to 152.78.177.66. Redistribution subject to AIP license or copyright; see http://jap.aip.org/about/rights_and_permissions

eliminates the first possibility. The second possibility is eliminated in favor of particle oscillation by two observations: (1) Particle distributions do show a strong bias towards the ends of the radial range (Fig. 4) and (2) particles have been observed to comeback at radial maxima-minima positions at regular frequency that depends upon their diameter and the flow Reynolds number. In fact, the sharp frequency peaks (in fundamental, i.e., f_1 and its integral multiplication modes, e.g., $2f_1$) in the frequency spectra of Fig. 3 further strengthen the second argument. If particles were just confined within a finite range without performing an oscillatory movement, such peaks in frequency spectra would not have appeared.

In spite of the elaborate dissection of experimental results, the fundamental origin of the oscillatory nature itself remains unclear. Towards this end, we have attempted to flush out the important parameters that control the dynamics of particle oscillation (Figs. 5 and 6). With this goal in view, we have mapped the distribution of lateral positions of embolic beads with the variation in flow Reynolds number and hematocrit level. To understand the underlying dynamics further and for sake of simplification, here, we delineate these trends particularly for particles with small α, i.e., low degree of confinement ($\alpha = 0.05 \pm 0.01$), and large α, i.e., high degree of confinement ($\alpha = 0.3 \pm 0.01$). Consequently, from these additional studies, three interesting points emerge: (a) oscillatory behavior is exhibited only by the beads with large diameter, i.e., high degree of confinement (Fig. 5(b)), (b) even with large beads, oscillation occurs only in the presence of high hematocrit level ($\geq 20\%$) and in relatively high flow Reynolds number (Figs. 6(a) and 6(b), and (c) the critical *Re* at which the oscillation begins, decreases with increasing hematocrit level. In the absence of RBCs, with increasing *Re*, we observed that the particles were trivially pushed towards the channel wall, without any hint of lateral oscillation (Fig. 5(a)). It is important to note that, in the absence of RBC, the effect of increase in *Re* is more pronounced for smaller particles than the larger ones (Fig. 5(a)). Presence of significant RBC fraction ($H_c = 40\%$) in the flow medium, however, considerably changes the scenario (Fig. 5(b)). In this case, while smaller particles tend to show unperturbed centrifugal trend with increasing *Re*, for larger particles an oscillatory dynamics sets in beyond a threshold Reynolds number which lies between 10 and 12 (Fig. 6(b)). Next, when we varied the haematocrit level ($H_c = 0\%$, 10%, 20%, 30%, and 40%) and performed the same set of experiments, we found that this critical *Re* magnitude

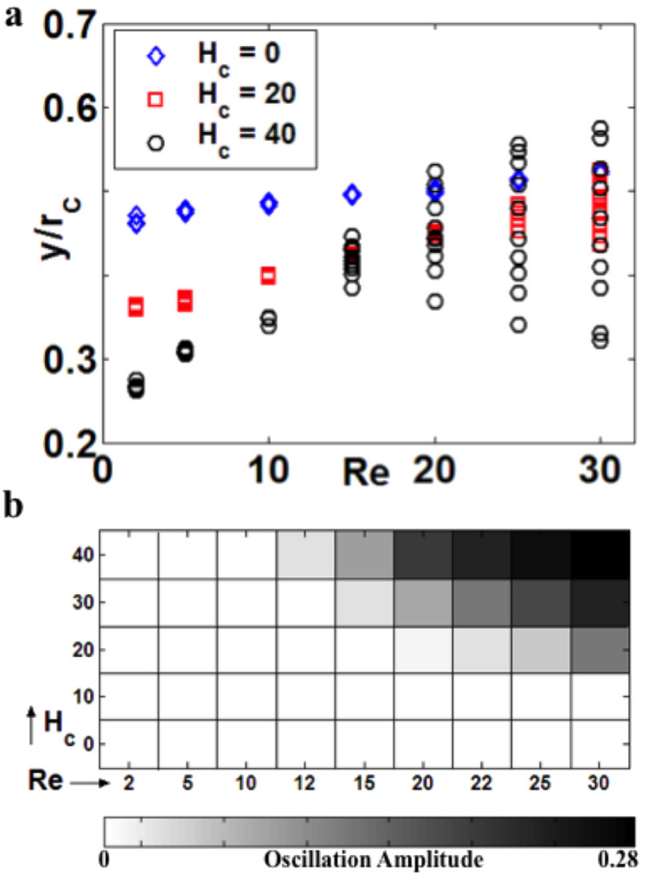

FIG. 6. Combined effect of flow Reynolds number and hematocrit level. (a) Dependence of lateral migration on flow Reynolds number at different H_c levels, for $\alpha = 0.3 \pm 0.01$. At least five independently acquired data points have been plotted for each *Re* value. (b) Variation in average oscillation amplitude (normalized by channel diameter) of microspheres with $\alpha = 0.3 \pm 0.01$ in the parametric-space of *Re* and H_c.

depends upon the hematocrit level (Fig. 6(b)). In general, it can be commented that critical Reynolds number (Re_{cr}) decreases with increasing H_c, but we could not establish any analytical relationship between these two parameters. It was also observed that within the scope and the range of current experiments, hematocrit levels lower than 20% were unable to elicit lateral oscillation (Fig. 6(b)).

The above experimental observations suggest the existence of a complex interplay between the governing physical parameters in determining the wide range of particle dynamics described here. Notably, the governing physics includes fluid rheology, fluid inertia, and particle relative dimension

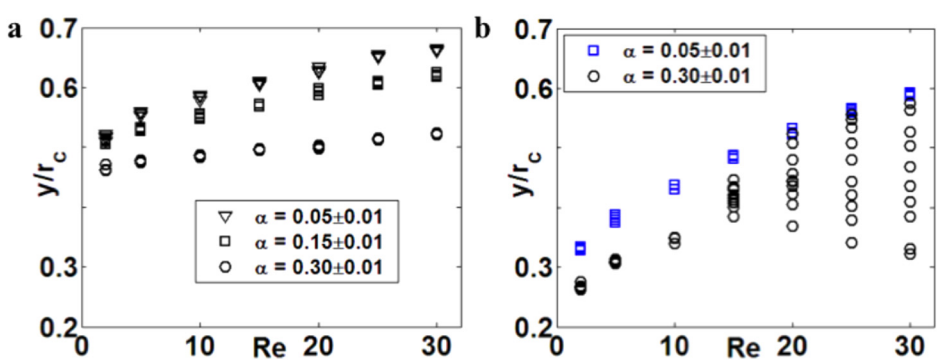

FIG. 5. Dependence of lateral migration on flow Reynolds number: (a) for $H_c = 0\%$ and (b) for $H_c = 40\%$. At least five independently acquired data points have been plotted for each *Re* and α. For $H_c = 40\%$, larger microspheres ($\alpha \sim 0.3$) show oscillating dynamics if $Re \geq 12$.

Downloaded 18 Dec 2012 to 152.78.177.66. Redistribution subject to AIP license or copyright; see http://jap.aip.org/about/rights_and_permissions

(e.g., degree of confinement). In an attempt to elucidate the nature and mutual contribution of the mechanisms leading to beads oscillation, a qualitative analysis is adopted here. First, the observed lateral migration of particles suspended in a RBC-free fluid flow ($H_c = 0\%$) depends on the mutual contribution of a "shear-gradient" lift and a "wall-effect" lift, as clearly illustrated by Di Carlo and co-workers for a Newtonian background flow in micro-confinement.[13,14,18] In this scenario, the experimental observations illustrating *Re*- and α-dependence of beads equilibrium position and axial velocity (Fig. 2) further corroborate the previous investigations.[14,18] Analogous considerations do apply for the flow behavior of particles suspended within relatively diluted RBC suspensions ($H_c \leq 10\%$), for which the governing physics can be explained within the Newtonian paradigm, since fluid viscosity is virtually invariant with respect to the shear rate at these low hematocrit levels.[24,25,28] Conversely, at higher hematocrits ($H_c \geq 20\%$), the non-Newtonian nature of blood cannot be neglected and fluid viscosity varies with the fluid shear rate.[25,28] With this respect, we have considered blood as a viscoelastic fluid which manifests shear-thinning behaviour (i.e., the apparent viscosity decreases with increasing the shear rate; as manifested from the plausible values of the Power Law index to be less than unity), considering previous investigations on blood flow within arteries.[25,29] This behavior influences a distinctive lateral variation in the velocity field as compared to that of a Newtonian fluid. It is also important to mention in this context that analogous to the observations of Sullivan *et al.* on the motion instability of bubbles in viscoelastic flows,[22] the oscillation of suspended particles can be conceptualized as the effect of a perturbing force which displaces the particle from an unstable transverse equilibrium position. Notably, particle motion and lateral position are governed by the competitive action of inertia and the effect of compressive normal stresses originating from the viscoelastic properties of the RBC suspensions. Elastic normal stresses have been observed to push the suspended particles towards the nearby wall, even in inertia-free flows (e.g., no equilibrium position is attained in this specific scenario).[30–33] Furthermore, in viscoelastic flows of suspended spherical particles, either inertial effects or normal stresses have been observed to be strongly influenced by the degree of confinement and the rheological properties of the fluid (e.g., level of shear thinning).[30,31] At $H_c \geq 20\%$, beads were observed to attain an equilibrium lateral position up to a critical Reynolds number (Re_{cr}) (Fig. 6), with the transverse location of the bead being likely to be determined by the competitive contribution of inertial lift and elastic normal stresses, as illustrated by Huang and co-workers.[31] However, such equilibrium condition can be perturbed by the effect of fluid shear thinning (perturbing force or agent), which enhances the magnitude of compressive normal stresses at places of higher shear rate and thus strengthens bead attraction towards the channel wall.[31] Consequently, at a given *Re* and haematocrit $\geq 20\%$, when the effect of shear thinning is strong enough to elicit a perturbation of the force field (conforming to a critical hematocrit level, $H_{c,cr}$), beads are displaced from their equilibrium position and start to oscillate under the effect of competing inertial forces and elastic normal stresses. This explains why the oscillation magnitude increases with increasing the Reynolds number (signifying higher inertia) and the hematocrit level (signifying higher elastic normal stresses), once the equilibrium position has been lost (see Figs. 6(a) and 6(b)). Furthermore, increasing the degree of confinement (e.g., higher α) leads to an intensification of the compressive normal stresses which directs the particles towards the wall,[31] and this contribution further reinforces the effect of shear thinning in destabilizing the transverse equilibrium of the bead. This will be particularly enhanced in higher *Re* regimes, due to beads attaining a more peripheral transverse location, and explains why the onset of oscillation at the higher *Re* occurs at lower hematocrit levels. This, interestingly, suggests a synergistic implication of confinement and shear thinning in triggering bead oscillations, as aggravated by more prominent shear thinning effects being induced at high hematocrit levels. Enhanced shear thinning effects (corresponding to higher hematocrit levels) are, thus, required to elicit bead oscillation at relatively lower Reynolds numbers (Fig. 6). Conversely, at lower degree of confinement (e.g., $\alpha < 0.15$), beads suspended in viscoelastic fluid flow have been observed to experience a lateral force directed towards the center of channel,[31] which differentiates from the larger beads and counteracts the effect of shear thinning. This essentially suggests a competitive effect of confinement and shear thinning in triggering the bead oscillations, at lower values of α. This is likely to prevent smaller beads from oscillating within the range of Reynolds numbers investigated here (Figs. 5 and 6), and explains why transverse oscillations in the bead could be detected only above a critical level of confinement (Fig. 2).

IV. CONCLUSIONS

In this study, we show that in the presence of RBCs, embolic microspheres may undergo lateral oscillations in narrow confinements, with unique dynamical characteristics, bearing significant implications on embolization based cancer therapy. Our experimental results reported here, expressed in terms of relevant dimensionless parameters, may have multifarious implications. First of all, these suggest that the embolisation location should be determined by the smaller microspheres in the mixed population as the axial migration velocity falls with increasing d_p, which is counter-intuitive to what is conventionally believed in embolization therapy and congruent to observations.[1,3,7] Second, beyond embolization, particle dynamics in RBC suspension can be important for the proper functioning of immune-surveillance cells such as neutrophils which are themselves microspherical in shape. It has been known that blood velocity and RBC concentration are important factors affecting the localization and binding of neutrophils to pathogens and blood-vessel wall constituting endothelial cells. However, it remains elusive how exactly the blood flow plays its part. The present investigation kindles the fluid dynamics perspective of such physiological events. Third, from practical considerations, the phenomena of lateral oscillations and slowing down of larger particles can be used as a method to

Downloaded 18 Dec 2012 to 152.78.177.66. Redistribution subject to AIP license or copyright; see http://jap.aip.org/about/rights_and_permissions

engineer a band-pass inertial particle separator without requiring an embedded matrix for differential migration. Finally, a further question remains on whether such oscillatory dynamics could originate in entangled polymer and shear banded flows.[34–36] If probed, such investigation would facilitate new developments in microfluidic systems with complex fluids.[22,23] It, however, needs to be mentioned that in the present study, we neglect the pulsatility of blood flow and deformable nature of arterial wall which may not be significant in arteries but may lead to interesting results in other circumstances. We are currently working on these aspects.

ACKNOWLEDGMENTS

Authors sincerely thank Biocompatibles UK Ltd., for providing embolic microbeads. This document is an output partially from the UK-India Education and Research Initiative (UKIERI) program (Project Code: SA08-086) funded by Department of Business, Innovation and Skills (BIS), Foreign and Commonwealth Office (FCO), British Council, Welsh Assembly Government and the Ministry of Human Resource Development (MHRD), Government of India.

[1]B. Morgan, A. S. Kennedy, V. Lewington, B. Jones, and R. A. Sharma, Nat. Rev. Clin. Oncol. **8**, 115–120 (2011).
[2]N. H. Nicolay, D. P. Berry, and R. A. Sharma, Nat. Rev. Clin. Oncol. **6**, 687–697 (2009).
[3]M. Vente, B. Zonnenberg, and J. Nijsen, Expert Rev. Med. Devices **7**, 581–583 (2010).
[4]D. Carugo, L. Capretto, S. Willis, A. L. Lewis, D. Grey, M. Hill, and X. Zhang, Biomed. Microdevices **14**, 153–163 (2012).
[5]R. López-Benítez, G. M. Richter, H.-U. Kauczor, S. Stampfl, J. Kladeck, B. A. Radeleff, M. Neukamm, and P. J. Hallscheidt, Cardiovasc. Intervent. Radiol. **32**, 615–622 (2009).
[6]A. L. Lewis and M. R. Dreher, J. Controlled Release **161**, 338–350 (2012).
[7]A. Laurent, Tech. Vasc. Interv. Radiol. **10**, 248–256 (2007).
[8]J. Bruix, M. Sala, and J. M. Llovet, Gastroenterology **127**, S179–S188 (2004).
[9]A. L. Lewis, M. V. Gonzalez, S. W. Leppard, J. E. Brown, P. W. Stratford, G. J. Phillips, and A. W. Lloyd, J. Mater. Sci.: Mater. Med. **18**, 1691–1699 (2007).
[10]J. Kettenbach, A. Stadler, I. Katzler, R. Schernthaner, M. Blum, J. Lammer, and T. Rand, Cardiovasc. Intervent. Radiol. **31**, 468–476 (2008).
[11]A. Lewis, C. Adams, W. Busby, S. Jones, L. Wolfenden, S. Leppard, R. Palmer, and S. Small, J. Mater. Sci.: Mater. Med. **17**, 1193–1204 (2006).
[12]I. Sakamoto, N. Aso, K. Nagaoki, Y. Matsuoka, M. Uetani, K. Ashizawa, S. Iwanaga, M. Mori, M. Morikawa, and T. Fukuda, Radiographics **18**, 605–619 (1998).
[13]D. Di Carlo, J. Edd, K. Humphry, H. Stone, and M. Toner, Phys. Rev. Lett. **102**, 94503 (2009).
[14]D. Di Carlo, D. Irimia, R. G. Tompkins, and M. Toner, Proc. Natl. Acad. Sci. U.S.A. **104**, 18892–18897 (2007).
[15]N. Al Quddus, W. A. Moussa, and S. Bhattacharjee, J. Colloid Interface Sci. **317**, 620–630 (2008).
[16]B. Chun and A. Ladd, Phys. Fluids **18**, 031704 (2006).
[17]J. P. Matas, J. F. Morris, and E. Guazzelli, J. Fluid Mech. **515**, 171–195 (2004).
[18]D. Di Carlo, Lab Chip **9**, 3038–3046 (2009).
[19]D. Di Carlo, F. Jon, D. Irimia, R. G. Tompkins, and M. Toner, Anal. Chem. **80**, 2204–2211 (2008).
[20]J. M. Martel and M. Toner, Phys. Fluids **24**, 032001 (2012).
[21]K. J. Humphry, P. M. Kulkarni, D. A. Weitz, J. F. Morris, and H. A. Stone, Phys. Fluids **22**, 081703 (2010).
[22]M. T. Sullivan, K. Moore, and H. A. Stone, Phys. Rev. Lett. **101**, 244503 (2008).
[23]T. Beatus, T. Tlusty, and R. Bar-Ziv, Nat. Phys. **2**, 743–748 (2006).
[24]D. J. Schneck and C. L. Lucas, *Biofluid Mechanics* (New York University Press, New York, 1990).
[25]G. P. Galdi, R. Rannacher, A. M. Robertson, and S. Turek, *Hemodynamical Flows: Modeling, Analysis and Simulation* (Birkhäuser, 2008).
[26]See supplementary material at http://dx.doi.org/10.1063/1.4768889 for [A] Power Law model for blood rheology; [B] determination of the Reynolds number; and [C] detection of bead position and quantification of bead velocity.
[27]G. Segre, Nature **189**, 209–210 (1961).
[28]M. Anand and K. Rajagopal, Int. J. Cardiovasc. Med. Sci. **4**, 59–68 (2004).
[29]B. M. Johnston, P. R. Johnston, S. Corney, and D. Kilpatrick, J. Biomech. **37**, 709–720 (2004).
[30]G. D'Avino, P. L. Maffettone, F. Greco, and M. Hulsen, J. Non-Newtonian Fluid Mech. **165**, 466–474 (2010).
[31]P. Huang, J. Feng, H. H. Hu, and D. D. Joseph, J. Fluid Mech. **343**, 73–94 (1997).
[32]G. D'Avino, G. Cicale, M. Hulsen, F. Greco, and P. L. Maffettone, J. Non-Newtonian Fluid Mech. **157**, 101–107 (2009).
[33]B. Ho and L. Leal, J. Fluid Mech. **76**, 783–799 (1976).
[34]P. Nghe, S. Fielding, P. Tabeling, and A. Ajdari, Phys. Rev. Lett. **104**, 248303 (2010).
[35]S. M. Fielding and H. J. Wilson, J. Non-Newtonian Fluid Mech. **165**, 196–202 (2010).
[36]S. Fielding and P. Olmsted, Phys. Rev. Lett. **90**, 224501 (2003).

Downloaded 18 Dec 2012 to 152.78.177.66. Redistribution subject to AIP license or copyright; see http://jap.aip.org/about/rights_and_permissions